Supplementary Online Material

Extended discussion of all the points raised here can be found in Ref. 1.

Sample fabrication

The samples were fabricated using double angle shadow evaporation through a single suspended resist mask prepared by standard e-beam lithography. To ensure a clean contact between the silver and aluminum layers, the two metals were evaporated during the same pump-down, in a ~10^{-4} Pa vacuum. First, a 30 nm-thick layer of Ag was deposited, immediately covered by a 2nm-thick layer of Al, both deposited under the same angle (17°). Then a second layer 60 nm-thick of Al was deposited at a different angle (-17°). The surface of the aluminum layers gets oxidized over typically 4nm when removing the sample from the vacuum system. The mask and the evaporation angle were such that the shift between the two images was large enough for the Al loop not to touch its parasitic Ag image at any point. This prevents any weakening of superconductivity at spots in the Al loop. Figure S1 shows scanning electron micrographs (SEM) of the four structures for which the low temperature AFM images taken during the experiment are shown in Fig. 2 of the Letter. The SEM images were taken after the low temperature measurements were completed.

Phase bias

The total magnetic flux threading the loop determines the integral of the gauge-invariant phase gradient around the complete loop (see M. Tinkham, *Introduction to Superconductivity*, McGraw-Hill,New York, 1985). In our samples the size of the loop is designed small enough for its geometrical inductance L_G and therefore the screening flux to be negligible. Consequently the total magnetic flux corresponds essentially to the external flux. Furthermore, the superconducting part of the loop is made wider and thicker than the normal one so that its kinetic inductance $L_S = \frac{1}{\pi} R_S \frac{\hbar}{\Delta}$ is much smaller than the one $L_N \simeq R_N \frac{\hbar}{\delta}$ of the proximity superconductor (here R_S is the normal state resistance of the S wire, R_N the resistance of the normal wire, and δ its minigap). For a given circulating supercurrent J in the loop, the phase difference $L_S J$ accumulated along the S part is therefore small as compared to the one $L_N J$ across the N part. Under these conditions the net result of an applied flux ϕ is essentially to induce a phase difference $\varphi = 2\pi\phi/\phi_0$ across the N wire, within

correcting factors of the order $(L_S + L_G)/L_N$. For our samples these corrections are always smaller than 10%.

Experimental setup

We show in Fig. S2 a 3D CAD scheme of the microscope assembly and a photograph of the microscope mounted on the cold plate of the inverted dilution refrigerator [2], with all the wiring connected. Figure S3 shows the dual mode sensor assembly details. The tuning fork used as AFM sensor is Ref. DS26-L2N from MICRO CRYSTAL. The tip is made out of a 25 µm diameter tungsten wire. As bulk tungsten becomes superconductor only below 15 mK, we consider it as a normal metal in this work, with a constant density of states in the relevant energy range.

In practice, vibrations generated by the helium circulation in the refrigerator limited the mechanical stability of the setup and hindered acquiring tunneling spectroscopy data with a true vacuum gap, as normally achieved in STMs. Laying the tip onto the thin oxide layer deposited on the sample allows circumventing this stability problem. Hence, our tunneling measurements actually bear more similarities with those made in planar tunnels junctions than those in standard STMs. Remarkably, in our measurements we find no visible trace of the properties of the barrier, of contamination laying on it, or of details regarding the tip apex. This contrasts with most STM spectroscopic measurements which are found very sensitive to contamination and tip shape. We think the reason for this difference is that the energy range probed in usual STM spectroscopy typically extends over a few volts, a scale on which the contaminants have an energy-dependent behavior, whereas, in our case, since the we only explore a tiny energy range (~1 mV), we don't see these variations and contaminants only change the barrier transparency.

Proximity effect modeling

Computing the LDoS in our structures requires, in principle, to specify their full 3-D geometry (including the interfaces and their properties) and to solve the Usadel equations [3,4] for this geometry. This complex task would require the input of many sample parameters not readily accessible, and has never been done. We restrict here to solving a much simpler one-dimensional model, as is generally done for SNS structures [4-6]. By using this model we essentially give up describing correctly the neighborhood of the nominally 50 nm-long overlap junctions between Ag and Al, and we assume that the dimensions transverse to the structure (*i.e.* film thickness and width) are smaller than the superconducting coherence length so that the LDoS can be assumed uniform along them. This latter assumption is well justified in the Ag wires but only marginally valid for the

width of the aluminum loops. Hence, we do not expect the predictions of this simplified model to fit the results of the experiment in a detailed fashion.

In this simplified model the parameters are: the gap of aluminum, the diffusion constant in the materials and their cross-sections, the effective length of the N wire, the phase difference across the wire, and, for each interface, the interface resistance and a parameter characterizing the distribution of transmission eigenvalues of its scattering matrix. Out of these parameters, the gap of Al, the phase difference, the cross sections and the wire length are known independently. The remaining free parameters are the diffusion constant in Al and Ag taken to be the same for all samples and, in principle, two interface parameters for each side of each wire. However, when trying to reproduce the observed LDoS at the various positions along the structures, it appears that some features (like the dip appearing in the proximity LDoS at the voltage corresponding to the bulk Al gap) are best reproduced if the interfaces transmission eigenvalues are close to 1. This is consistent with having evaporated the Al and Ag layers in the same vacuum, thus forming a good contact. By setting the transmission eigenvalues to 1 for simplicity, we reduce the number of fitting parameters to two for each wire, i.e. the two interface resistances. These interface resistances are finite even though the channel transmission is unity, each open channel contributing to the interface conductance with twice the conductance quantum e^2/h. Given the wire cross section, the maximum number of open channels is ~22000, which yields a minimum interface resistance of 0.6 Ω.

In principle, the reduction of the local superconducting order parameter on an S electrode close to an NS interface should derive from a self-consistent resolution of the Usadel equations. However, we expect this effect to be small in our samples because the S cross section is nominally 8 times larger than the N one. Here, since we are looking only for a qualitative model capable of rendering the main features of the data, we avoided this extra complication and manually set slightly reduced order parameters on either side of the N wires (See Table S1). These parameters are tightly constrained however, because they determine the position of the peak in the LDoS for measurements taken on the S sides close to the interfaces. Not adjusting these order parameter values would slightly degrade the agreement shown in the figures, but would not change qualitatively the shape of the calculated LDoS.

Furthermore, as already explained in the Letter, due to the finite extension of the overlap interfaces of N and S in the samples, one cannot define exactly the tip-to-interface distance. In particular, when the tip is apparently at one end of the N wire on the AFM image, it is still at an *average* distance of all points of the interface equal to half the overlap length. Hence, for simplicity, the effective position of the tip along the effective N wire length in the model is crudely mapped to the apparent position of the tip on the AFM image, taking into account this offset. A similar offset

occurs on the S side, where one needs to take into account the thickness of the Al film.

Finally, we have found that for some positions around the interfaces the overall shape of the measurements are better reproduced with a slight additional offset of the effective position of the tip. This is probably related to a deformation of the tip after repeated contact with the sample or to the non-uniform cross-section of the wires visible in the micrographs shown in Fig. S1.

FIGURES

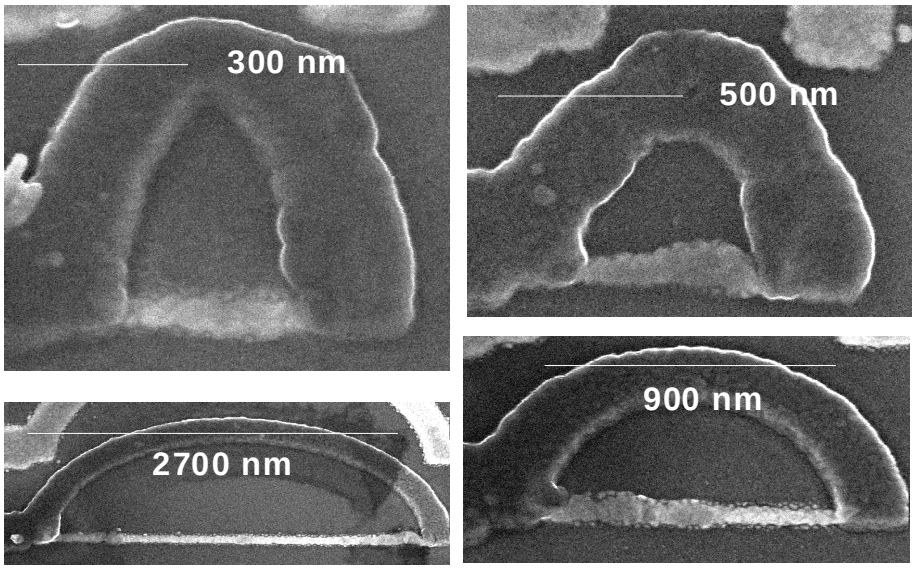

Figure S1. Scanning electron micrographs of the structures measured during this experiment. The darker metal is Al, and the lighter Ag.

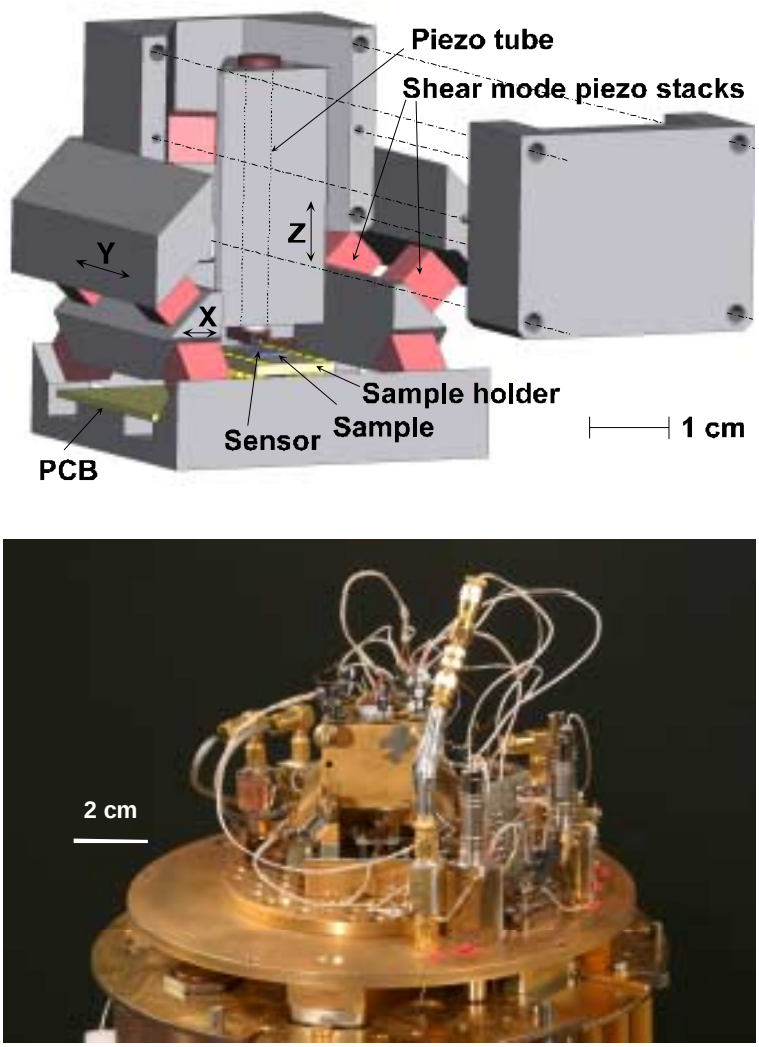

Figure S2. Top : CAD image of the microscope. For clarity, one of the parts holding the vertical (z) sliding part is shown unattached. It is normally gently pressed against the z moving part by screws and springs. Three orthogonal mating prismatic shapes are used to guide sliding parts which provide coarse positioning of the sensor tip above the fixed sample. The sliding parts are actuated by inertial stick-slip motion of four shear-mode piezoelectric stacks for each axis. The fine scanning of the sample surface by the sensor tip is done by a piezoelectric tube enclosed in the z moving part. Bottom: the microscope is shown here mounted on the coldest plate of the inverted dilution refrigerator.

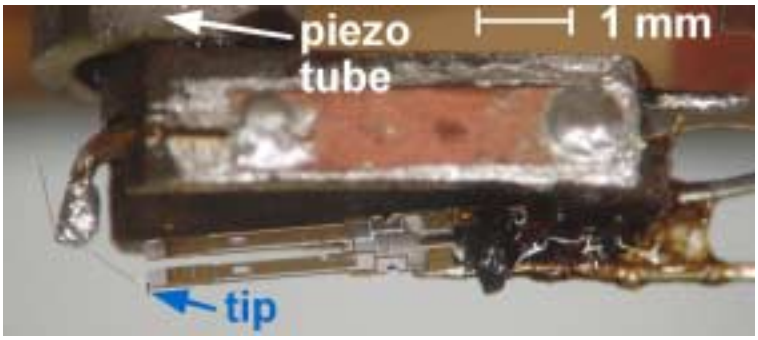

Figure S3. The dual-mode STM-AFM sensor. The sensor consists of a tungsten tip glued on a miniature quartz tuning fork, itself mounted on a stand at the extremity of the piezoelectric scanning tube. The visibility of the tip was enhanced on this picture. The tip is formed by electrochemically etching a 25 µm diameter tungsten wire. It is then cut and glued using silver epoxy to the lower prong of the quartz tuning fork. The tunnel current is carried by a 25 µm-diameter gold wire also glued to this prong [8].

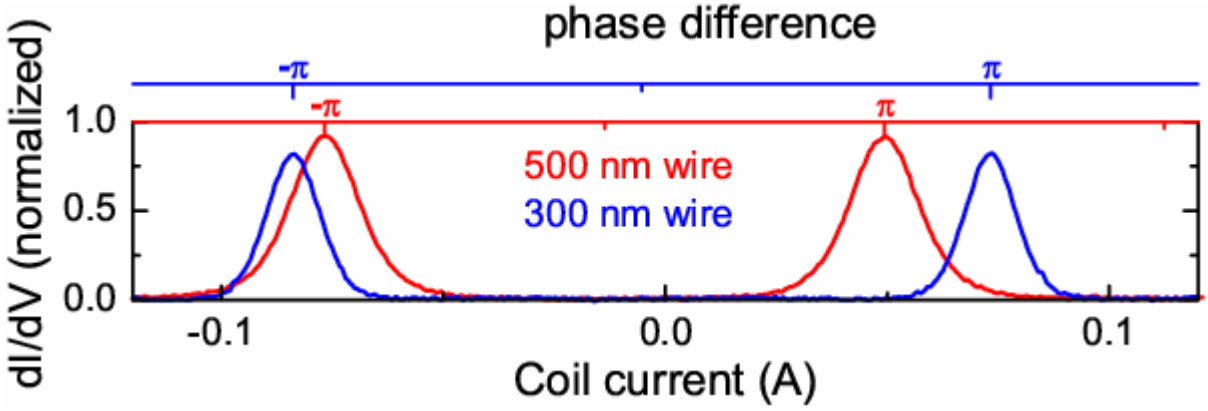

Figure S4. Phase dependence of the differential conductance in the middle of two Ag wires (300 and 500 nm long) measured by varying the magnetic field perpendicular to the loop. The phase calibration is obtained from this measurement. In practice, the number of periods that can be spanned is limited to three or four because, as the loops are very small, a flux quantum corresponds to a sizeable fraction of the critical field of the thin Al film.

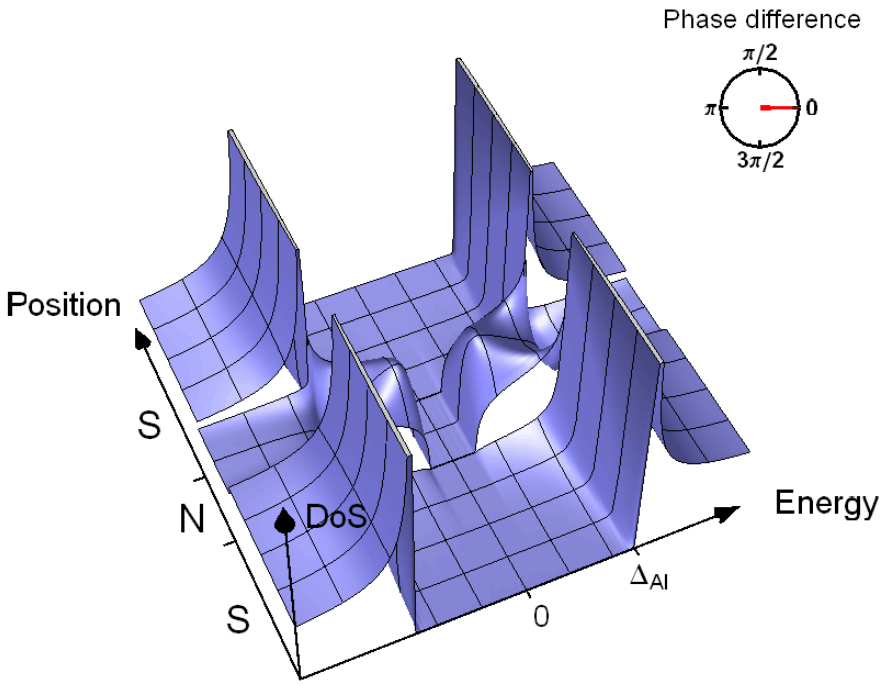

To play this animation, please see the ‘‘Animation_S1.avi” file

Animation S1. This animation shows the evolution of the LDoS plotted in Figure 1 of the Letter when the superconducting phase difference across the structure is varied. This shows the periodic behavior of the LDoS and the vanishing of the minigap around $\varphi = \pi$. Each division along the position axis corresponds to a coherence length ξ.

		Structure 1 “300 nm wire”	Structure 2 “500 nm wire”	Structure 3 “900 nm wire”	Structure 4 “2700 nm wire”
Apparent length (nm)		307	430	870	2550
Effective length ℓ (nm)		350	550	950	2750
Diffusion constant D (cm^2s^{-1})		170			
Gap energy (μeV) (left;right)		160	170;173	175	170
Left interface	average τ	1			
	r_L ratio	0.7	4.0	0.5	1.0
Right interface	average τ	1			
	r_R ratio	0.5	0.05	2.0	0.6

Table S1. Input parameters to the 1-D model used to describe the data. The apparent length of each wire is the measured length of the visible part of the N wire on the SEM pictures shown in Fig. S1. The effective length, which is the one actually used in the 1D model, is larger than the apparent length to take into account the overlap geometry of the interfaces. It was taken equal to the designed visible length plus half the sum of the two overlaps as measured from the AFM images. The average channel transmission τ was set to 1 for all interfaces. The left and right interfaces resistances $R_{L,R}$ (which are inversely proportional to the number of open channels at each interface) are specified here as the ratios $r_{L,R} = R_{L,R}/R_\xi$ to the resistance $R_\xi \sim 4\Omega$ of the wire on a coherence length $\xi = \sqrt{\hbar D/\Delta} \sim 250\,\mathrm{nm}$. The reduction of the order parameter on either side of the wires due to the inverse proximity effect is here taken into account by adjusting the energy gap to fit the position of the peak in the LDoS.

References for Supplementary Online Material

1 H. le Sueur, PhD Thesis (in English), Université Paris 6, 2007. Available online at http://tel.archives-ouvertes.fr/tel-00261434/en/

2 The inverted dilution refrigerator (called “Sionludi”) was designed by A. Benoît, and M. Caussignac, at CNRS-Grenoble.

3 K.D. Usadel, Phys. Rev. Lett. **25**, 507 (1970).

4 W. Belzig, F.K. Wilhelm, C. Bruder, G. Schön, and A.D. Zaikin, Superlatt. and Microstruct. **25**, 1251 (1999).

5 J.C. Hammer, J. C. Cuevas, F.S. Bergeret, and W. Belzig, Phys. Rev. **B 76**, 064514 (2007)

6 J.J.A. Baselmans, T. T. Heikkilä, B. J. van Wees, and T. M. Klapwijk, Phys. Rev. Lett. **89**, 207002 (2002).

7 J.G. Rodrigo *et al*, J. Phys.: Condens. Matter **16,** R1151 (2004).

8 Ihn, T. *et al*, arXiv:cond-mat/0112415, (2001).